Interband Tunneling Transport in 2-Dimensional Crystal Semiconductors

Nan Ma and Debdeep Jena

Department of Electrical Engineering, University of Notre Dame, Notre Dame, IN 46556

Email: nma@nd.edu/ Phone: (574)855-6360

Interband quantum tunneling of electrons in semiconductors is of intense recent interest as the underlying transport mechanism in tunneling field-effect transistors (TFETs). The emergence of 2-dimensional (2D) semiconducting crystals[1] provides a new material platform for realizing such devices. To date, interband tunneling in purely 2D semiconducting crystal junctions has not received sufficient attention, certainly not to the extent it has for 3D semiconductor p-n junctions since Zener's[2] and Esaki's works[3]. In this work, we derive an analytical expression for the Zener tunneling current in a 2D crystal semiconductor *p-i-n* junction. Using this expression, we evaluate various 2D crystal semiconductors for their tunneling current drives.

A 2D crystal *p-i-n* junction is shown schematically in Fig. 1 (a) with ohmic contacts to the *p*- and *n*-doped regions. The doping in the *p*- and *n*-sides aligns the Fermi levels to the respective band-edges. Under the application of a reverse bias voltage V, a finite tunneling window is created for electrons [Fig. 1(b)]. The tunneling probability, which is obtained by the Wentzel-Kramers-Brillouin (WKB) approximation[4], is lowered *exponentially* with their transverse kinetic energy as a consequence of lateral momentum conservation in the tunneling process, as indicated in the semi-ellipse in the k-space in Fig. 2.

At temperature $T\rightarrow 0$ K, f_v-$f_c\approx 1$ for the energy window of current-carrying electrons. We track each state in the 2D k-space, their respective group velocities and their interband tunneling probabilities. Figure 2 shows the zero-temperature interband tunneling current spectrum resolved in the k-space for 2D $MoTe_2$. By summing the contributions from the individual k-states, we obtain an expression for the interband tunneling current per unit width (μA/μm) in a 2D crystal *p-i-n* junction to be

$$J_T^{2D} = \frac{q^2}{h}\left(\frac{g_s g_v T_0}{2\pi}\right)\sqrt{\frac{2m_v^*\bar{E}}{\hbar^2}} \times \left[\sqrt{\pi}\left(V-\frac{V_0}{2}\right)\mathrm{Erf}\left(\sqrt{\frac{V}{V_0}}\right)+\sqrt{\frac{V}{V_0}}\exp\left(-\frac{V}{V_0}\right)\right] \quad (1)$$

where g_s, g_v are spin and valley degeneracy, respectively, T_0, V_0 and $\bar{E}$ are parameters determined by the electric field F, the effective mass (m^*) and energy bandgap (E_g) of 2D crystals. For small reverse bias voltages $V<<V_0$, the tunneling current varies as $J_T^{2D}\sim V^{3/2}$ to leading order. For larger voltages when $V>>V_0$, the tunneling current depends linearly on the voltage according to

$$J_T^{2D} \approx \left[\frac{q^2}{h}\left(\frac{g_s g_v}{2\pi}\right)\sqrt{\frac{2\pi m_v^*}{\hbar^2}\cdot\frac{q\hbar F}{\sqrt{8m_R^* E_g}}}\times T_0\right]V. \quad (2)$$

When T is high, Fermi-Dirac distributions of electrons are considered. The interband tunneling current densities of various 2D crystals at T=4 K and 300 K are plotted as solid and dashed lines in Fig. 3 (a) respectively. The tunneling current of $MoTe_2$ and a 2D semiconductor crystal with E_g = 1.0 eV and $m^* = 0.1m_0$ as a function of the voltage at different T is shown in Fig. 3 (b) and (c). The parameters of 2D crystals are listed in Table I. All possibilities are included by treating m^* and E_g as independent material parameters, as shown in Fig 4 (a). As it is evident, there is a tradeoff in the choice of e m^* and E_g for maximizing the tunneling current. Fig 4(b) shows the current density as a function of m^* with E_g of 0.1 eV and 1.0 eV, respectively. For high-performance TFETs for digital switching applications, currents exceeding 100μA/μm are highly desirable. For 2D crystals semiconductors with E_g smaller than ~0.3 – 0.4 eV, a choice of a *higher* m^* will maximize the interband tunneling current, far exceeding typical transistor on-currents for high-performance switching. But for larger E_g, a *lower* m^* is more desirable. Suitable on/off ratios for applications will then guide the choice of materials. The results presented here are expected to be useful for compact modeling and device simulators.

[1]Q. H. Wang et al, Nature Nano. **7**, 699 (2012), [2]C. Zener, Proc. R. Soc. Lond. A.**145**, 523 (1934), [3]L. Esaki, Phys. Rev. **109**, 603 (1958), [4]A. C. Seabaugh and Q. Zhang, Proc. of the IEEE **98**, 2095 (2010)

978-1-4799-0814-1/13/$31.00 ©2013 IEEE

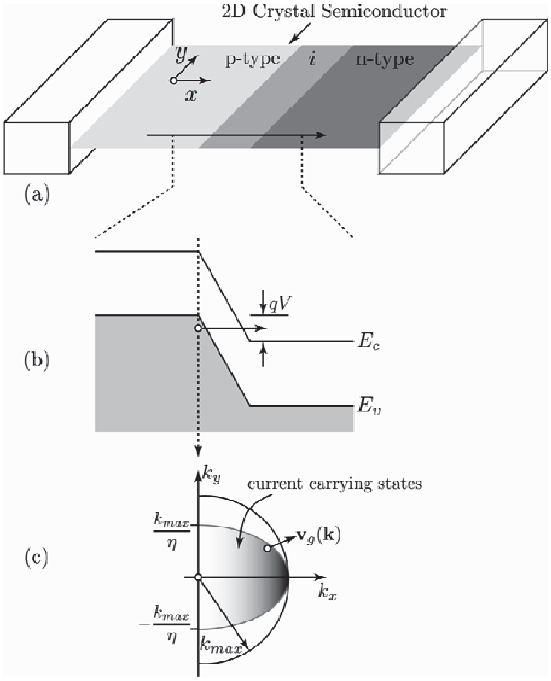

FIG. 1 Schematic depiction of a 2D crystal *p-i-n* junction (a), the energy band-diagram (b), and the **k**-space distribution of current densities. The **k**-states contributing to interband tunneling current and the group velocity are indicated.

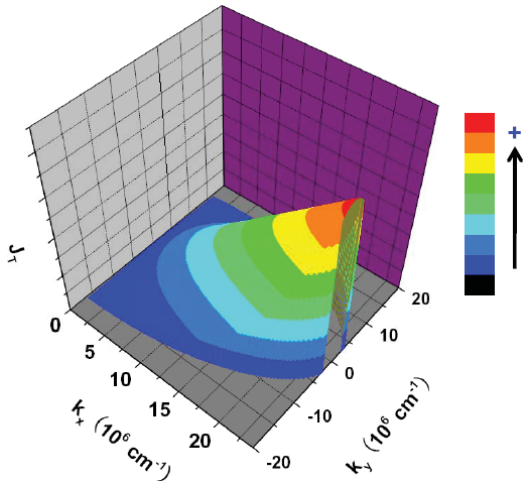

Fig. 2 Zero-temperature interband tunneling current spectrum resolved in the k-space in $MoTe_2$

	m_c^* (m_0)	m_v^* (m_0)	E_g (eV)
MoS_2	0.57	0.66	1.78
WS_2	0.34	0.45	1.93
$MoSe_2$	0.6	0.7	1.49
$MoTe_2$	0.61	0.75	1.13

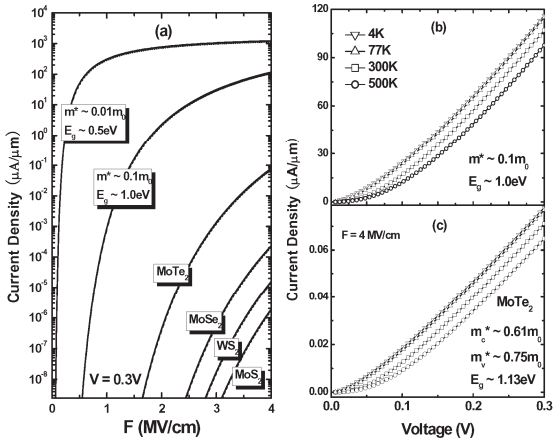

FIG. 3 (a) Interband tunneling current density for various 2D crystal semiconductors. The solid lines are at T=4 K, and the dashed lines at T=300 K, the temperature dependence is weak. (b) Current-voltage curves at various temperatures at a junction field F=4 MV/cm for a 2D crystal semiconductor with band parameters indicated. (c) Same as (b), but for the 2D crystal $MoTe_2$.

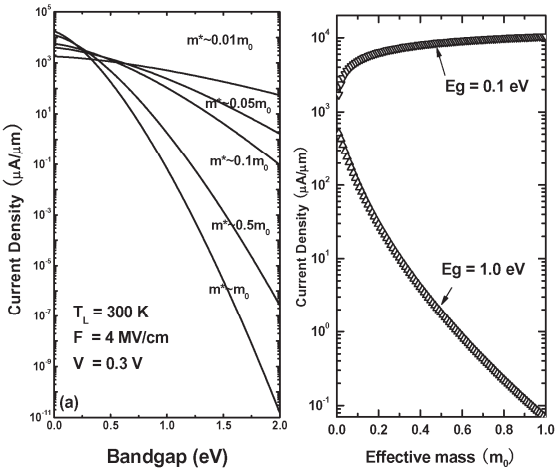

FIG. 4 (a) Interband tunneling currents for 2D crystal semiconductors as a function of the energy bandgap for various effective mass parameters. (b) The high current part of (a) zoomed in for more detail.

Table I: Conduction and valence band effective mass and bandgap of 2D crystals.

978-1-4799-0814-1/13/$31.00 ©2013 IEEE